https://doi.org/10.5194/esurf-2022-54
Preprint. Discussion started: 8 November 2022

Earth Surface Dynamics Discussions

Optimising global landscape evolution models with ^{10}Be

Gregory A. Ruetenik[1], John D. Jansen[1], Pedro Val[2], Lotta Ylä-Mella[1]

[1] GFÚ Institute of Geophysics, Czech Academy of Sciences, Prague, Czech Republic
[2] School of Earth and Environmental Sciences, Queens College, City University of New York, New York, USA
Correspondence to: Gregory A. Ruetenik (ruetenik@ig.cas.cz)

Abstract

By simulating erosion and deposition, landscape evolution models offer powerful insights to Earth surface processes and dynamics. These models are typically constructed from parameters describing drainage area (m), slope (n), substrate erodibility (K), hillslope diffusion (D), and a critical drainage area (A_c) that signifies the downslope transition from hillslope diffusion to advective fluvial processes. In spite of the widespread success of such models, the parameter values have high degrees of uncertainty mainly because the advection and diffusion equations amalgamate physical processes and material properties that span widely differing spatial and temporal scales. Here, we use a global catalogue of catchment-averaged cosmogenic ^{10}Be-derived erosion (denudation) rates with the aim to optimise a set of landscape evolution models via a Monte Carlo based parameter search. We consider three model scenarios: advection-only, diffusion-only, and an advection-diffusion hybrid. In each case, we search for a parameter set that best approximates erosion rates at the global scale, and we directly compare erosion rates from the modelled scenarios with those derived from ^{10}Be data. Optimised ranges can be defined for many LEM parameters at the global scale. In the absence of diffusion, $n \sim 1.3$, and with increasing diffusivity the optimal n increases linearly to a global maximum of $n \sim 2$. Meanwhile we find that the diffusion-only model somewhat outperforms the advection-only model and is optimised when concavity is raised to a power of 2. With these examples, we suggest that our approach provides baseline parameter estimates for large-scale studies spanning long timescales and diverse landscape properties. Moreover, our direct comparison of model-predicted versus observed erosion rates is preferable to methods that rely upon catchment-scale averaging or amalgamation of topographic metrics. We also seek to optimise K and D parameters in landscape evolution models with respect to precipitation and substrate lithology. These optimised models allow us to effectively control for topography and target specifically the relationship between erosion rate and precipitation. All models suggest a positive correlation between K or D and precipitation > 1500 mm yr^{-1}, plus a local maximum at ~ 300 mm yr^{-1}, which is compatible with the long-standing hypothesis that semi-arid environments are among the most erodible.

https://doi.org/10.5194/esurf-2022-54
Preprint. Discussion started: 8 November 2022

Earth Surface Dynamics Discussions Open Access EGU

1 Introduction

To appreciate short-term changes in Earth surface processes, such as those induced by humans (Brown, 1981; Hooke, 2000), it is first necessary to understand long-term rates of erosion and deposition. Recognizing this, some recent studies (e.g., Simoes et al., 2010) derive erosion-transport rules from topography with an aim to predict macroscale patterns of erosion and sediment flux. At more restricted scales, erosion rates based on cosmogenic nuclides (e.g., ^{10}Be) show a modest exponential correlation with catchment-averaged slope, as does normalised steepness in stream profiles (Portenga and Bierman, 2011; Harel et al., 2016). Nevertheless, it is widely observed that steepness and stream power parameters are subject to notable variation wherever climate and/or lithology differ (Harel et al., 2016; Gailleton et al., 2021; Marder and Gallen, 2022), and a robust analysis must accommodate such interactions.

Earth's surface undergoes continuous modification through uplift and erosion over timescales too long to observe directly, hence landscape evolution models (LEMs) are vital tools for building knowledge. LEMs are often employed over expansive scales of space and time in order to study topographic response to changes in tectonics (e.g., Kooi and Beaumont, 1996; Garcia-Castellanos et al., 2003), climate (Temme et al., 2009, Adams et al., 2020), and sea level (Pico et al., 2019; Ruetenik et al., 2019). And yet, large spatial and temporal scales require generalisation of model parameters that accounts reliably for processes of hillslope diffusion and advective fluvial erosion. Using LEMs to estimate erosion rates delivers the key advantage of bridging scales and defining an empirically derived mechanism at the local (grid cell) scale within each catchment. This demands that erosion rates are integrated over scales matching the topographic changes they describe. At the local to regional scale, recent studies have focused on constraining LEM parameters via inversions that optimise rates of erosion, deposition, and topographic observations (e.g., Miller et al., 2013; Croissant et al., 2014; Pedersen et al., 2018; Barnhart et al., 2020). However, implementing many of these approaches at a global scale is challenging in terms of both computational cost and because it often requires a compilation of a large set of observables (such as knickpoints, depositional patterns, and erosion rates). In the absence of computational power that can accurately model stratigraphy at the global scale, and without constraints on global palaeo-topography, we settle for optimising LEM parameters with respect to catchment-averaged erosion rates.

Here, we determine LEM parameter values that minimise the variance among ^{10}Be-derived apparent erosion rates in the *OCTOPUS* v.2 global catalogue (Codilean et al., 2022), and we analyse the capacity of LEMs to predict erosion rate given those optimised parameters. Our LEM employs the common stream power plus

https://doi.org/10.5194/esurf-2022-54
Preprint. Discussion started: 8 November 2022

diffusion formulation, which is subject to important limitations, such as the neglect of fluvial deposition and mass wasting processes (e.g., Whipple and Tucker, 1999). The trade-offs involved in this simplified approach, we believe, are justified by the record of success with simulating landscape processes at large scales and across a wide range of lithologies, drainage areas, and steepness (e.g., Gallen et al., 2013; Miller et al. 2013; Fox et al., 2014).

1.1 Catchment-averaged erosion rates from cosmogenic ^{10}Be

Rates of catchment-scale erosion can be estimated from abundances of cosmogenic radionuclides such as ^{10}Be, which is measured in quartz-bearing river sand (Granger et al., 1996; von Blanckenburg, 2005). Such nuclides accumulate within minerals exposed to secondary cosmic rays in the upper few metres of the bedrock subsurface and are lost via erosion and radioactive decay (Lal, 1991). The attenuation of cosmic rays with depth causes the nuclide production rate to decrease exponentially (at 2 m depth the ^{10}Be production rate is < 5 % that at the surface); hence, nuclide abundances measured in sediment are an inverse function of erosion (or, strictly denudation) rate.

The spatial variations observed in erosion rates across a range of climates and lithologies (Portenga and Bierman, 2011; Starke et al., 2020) suggest that the erosion processes driving the evolution of landscapes also vary. This has important implications for the interpretation of ^{10}Be-derived erosion rates and how we parameterize erosion in LEMs. Estimating catchment-averaged erosion rate from nuclide abundances in river sand depends on at least two fundamental premises (von Blanckenburg, 2005; Mudd, 2016): (1) sediments were produced via long-term, steady bedrock erosion distributed uniformly across the catchment; and (2) sediments have experienced continuous exposure to cosmic rays at/near the surface. In detail, long-term steady erosion refers to at least one attenuation length (~ 0.6 m) of erosion integrated over a 10^3–10^5 yr timescale. Hence, abrupt bedrock erosion events, for instance, caused by bedrock landsliding or glacial quarrying may bias erosion rate estimates. Similarly, long intervals of ice cover or intermittent deep sediment burial contradict the requirement for continuous cosmic-ray exposure. Other sources of potential discord relate to lithology, catchment size, and hypsometry, which are known to affect sediment transport dynamics and grain-size yields (Carretier et al., 2015; Riebe et al., 2015; Lukens et al., 2016; Zavala et al., 2020). The sources of deviation noted above are collectively responsible for the considerable variability observed in large compilations of ^{10}Be-derived erosion rates (e.g., Portenga and Bierman, 2011; Harel et al., 2016). Catchment-wide erosion rates are commonly determined and published for settings that do not comply strictly with the method's premises; these estimates are best referred to

https://doi.org/10.5194/esurf-2022-54
Preprint. Discussion started: 8 November 2022

as *apparent* erosion rates (Mudd, 2016). Nevertheless, ^{10}Be-derived erosion rates currently offer the most widely distributed insight into long-term, catchment-scale erosion rates on a global scale.

2 Methods

Stream power is represented by a non-linear advection equation derived from observations of river morphology and generalised relationships for bed shear stress (e.g., Howard et al., 1994; Whipple and Tucker, 1999; Lague, 2014). It affords a description of channel incision as a function of upstream drainage area (A) and local slope (S) for the portion of the catchment (above the critical drainage area, A_c) where fluvial advection dominates over hillslope diffusion and debris flow processes (e.g., Lague and Davy, 2003; Fontana et al., 2003; Whipple and Tucker, 1999). The stream power equation takes the form:

$$E_{predicted,advective} = K A^m S^n, \qquad (1)$$

where K is the advection coefficient or erosional efficiency, and m and n determine the relative dependence of incision on drainage area and slope. The ratio m/n defines the concavity of the longitudinal channel profile and typically varies from 0.3 to 0.6 (Wobus et al., 2006; Whipple and Tucker, 1999); n determines the erosional nonlinearity, which is thought to relate to regional flood variability and typically ranges from 1 to 4 (e.g., Lague, 2014). A global compilation of stream power parameters constrained by topographic metrics (Harel et al., 2016) reports an optimised $n \sim 2.6$. The value of n may also vary depending on the location in the channel network—the steepest and fastest-eroding locales such as knickpoints can have values closer to unity (Lague, 2014). In general, higher n results in larger erosional flux from steep terrain, while higher m results in larger flux from big rivers. However, if m and n both increase (keeping their ratio constant), a larger fraction of erosional flux will be sourced from steeper main-stem channels.

The amalgamated outcomes of hillslope transport processes, such as rainsplash, soil creep, and bioturbation, are primarily diffusive. Hence, to simulate hillslope processes, we include a diffusion equation:

$$E_{predicted,diffusive} = D\left(\frac{d^2 z}{dx^2} + \frac{d^2 z}{dy^2}\right)^p, \qquad (2)$$

https://doi.org/10.5194/esurf-2022-54
Preprint. Discussion started: 8 November 2022

where D is diffusivity, which is reported to range from ~ 4.4×10^{-4} to 3.6×10^{-2} for linear diffusion (e.g., Fernandes and Dietrich, 1997). We use a non-linear form of the diffusion equation in which concavity is raised to an exponent in order to harmonise with Gabet et al. (2021), which posits that erosion rate scales approximately with concavity squared. For linear diffusion, which is mass conservative, the deposited and eroded sediment should in balance. However, in the non-linear model, negative concavities raised to a power of p can produce non-real numbers. Thus, we produce an average catchment-wide erosion rate in which we ignore deposited sediment (areas of negative concavity) and take an average only based on eroded sediment in this model.

For our joint advection-diffusion model, we follow the common approach of combining stream power with linear diffusion (i.e., $p = 1$ in Eq. *2*). When Equations (*1*) and (*2*) are combined, D and K covary, and it has been noted that a higher D/K ratio results in a more linear scaling between erosion rate and catchment-averaged slope (Forte et al., 2016). Hence, we divide (Eq. *3*) by K, which allows the D/K ratio to be optimised with respect to predicted erosion rate:

$$\frac{E_{predicted}}{K} = A^m S^n + \frac{D}{K}\left(\frac{d^2 z}{dx^2} + \frac{d^2 z}{dy^2}\right), \quad (3)$$

With our advection-diffusion model formulation (Eq. *3*), we set out to solve simultaneously for globally optimised values of D/K, n and A_c. D/K and n determine the relative importance of advective versus diffusive processes in driving erosion; lower D/K and higher n (which implies higher m given uniform concavity) will result in the dominance of advection, whereas higher D/K and lower n will result in more diffusion-dominance. While varying m and n, we maintain their ratio constant at 0.45, a widely applied average channel concavity (e.g., Wobus et al., 2006; Harel et al., 2016), and in line with the global average of 0.42 reported by Gailleton et al. (2021).

Based on previous modelling results (e.g., Roering et al., 2007), one might expect advection-dominant landscapes to be rougher in outline relative to the smoothing effects of diffusion. However, Theodoratos et al. (2018) show that multiple sets of parameters can give rise to equifinality. In our modelling framework, the D/K ratio covaries with n to determine the ratio of hillslope erosion versus the total (fluvial + hillslope) erosion—denoted here as $E_{predicted,diffusive}/E_{total}$, where E_{total} is the sum of $E_{predicted,diffusive}$ and $E_{predicted,advective}$. The ratio $E_{predicted,diffusive}/E_{total}$ is therefore a function of both n and D/K. In principle, this metric is proportional to an (inverse)

5

https://doi.org/10.5194/esurf-2022-54
Preprint. Discussion started: 8 November 2022

Earth Surface Dynamics Discussions

effective Peclet number for net erosion (Perron et al., 2008). For values of $E_{predicted,diffusive}/E_{total}$ close to unity, diffusive processes will dominate, while values closer to zero represent advection dominance (Fig. 1).

2.1 ^{10}Be-derived apparent erosion rates

We conduct modelling experiments that employ randomly selected sets of LEM parameter values, and then compare our model outputs with the *OCTOPUS* v.2 global catalogue of ^{10}Be-derived catchment-averaged erosion rates (Codilean et al., 2022). In addition to apparent erosion rates (N = 4631), *OCTOPUS* includes topographic data and catchment morphometries. Using the catchment boundaries in *OCTOPUS*, we clipped rasters from the *Hydrosheds* Shuttle Radar Topography Mission (SRTM) dataset, a global digital elevation model (DEM) with 3-arc-second resolution (Lehner et al., 2008), plus the National Elevation Dataset (Gesch et al., 2002) for catchments in Alaska north of 60 degrees. Local pits (i.e., lakes) within the catchments were filled using the priority-flood method of Barnes et al. (2014). In building the network of local upstream drainage areas for each cell, runoff is assumed to flow down the steepest descent in accordance with the *D8* flow routing algorithm. Slopes for every cell are computed along this steepest-descent flow path.

To determine the effect of DEM resolution, we test our models on 1-arc-second SRTM data (Farr et al., 2004), although for reasons of computational capacity we restrict our analyses to catchments with < 13 million grid cells (N = 3414), and for the scenarios diffusion-only and advection-only. We find that DEM resolution is not pivotal (Appendix A, Fig. A1/A2).

About 24 % of the *OCTOPUS* dataset is not exploitable for our purposes: 91 catchments are too small to be processed by the LEM (< 3 DEM cells in any dimension), and we exclude 33 of the very largest catchments due to the extreme computational cost. Multiple erosion rate measurements included in *OCTOPUS* refer to samples from different locations within the same larger catchment. For such cases, a separate catchment is defined only where the drainage area differs by > 5 %; otherwise, we amalgamate the data and derive a single average erosion rate. In total, 3618 catchment-wide apparent erosion rates ($E_{apparent}$) are used in our modelling experiments, ranging from 0.028 km^2 to 129,000 km^2 (11 to 38 million grid cells). We do not separate ^{10}Be measurements conducted on different grain-size fractions.

After catchment slopes and drainage areas are computed, the diffusion and stream power equations can be solved. The LEM is run for exactly one time-step on DEMs representing each of the 3618 catchments; the sediment flux to the catchment outlet is then averaged over the total drainage area to yield a LEM-predicted erosion rate ($E_{predicted}$). Because different values of input LEM parameters typically yield different erosion rates

https://doi.org/10.5194/esurf-2022-54
Preprint. Discussion started: 8 November 2022

(with the exception of highly diffusive models, as described below), such models are then optimised by comparison with our catalogue of $E_{apparent}$ data.

2.2 Monte Carlo simulations

We use a brute-force Monte Carlo approach to investigate the parameter space by running randomly selected sets of parameters and testing the fit of modelled versus observed (^{10}Be-derived) erosion rates. We adopt the philosophy of equifinality (e.g., Beven and Binley, 1992) to evaluate the model parameters applied in our LEMs; implicit in these assumptions is that multiple sets of parameters may give rise to a similar, or equifinal, result (e.g., Csilléry et al., 2010). Hence, we report both the range of optimal parameters in addition to the best-fit model parameters.

In our framework, no more than three parameters are modified and compared at any one time (Table 1). This is possible thanks to several simplifying steps (detailed below) that require fewer modelling runs (e.g., Theodoratos et al., 2018). The performance of the model with a given set of parameters is evaluated based on the mismatch between $E^*_{predicted}$ and $E_{apparent}$ with respect to the likelihood function (Beven and Binley, 2014). Modelled and observed rates are compared directly, no regression is involved. In so doing, one or more local maxima representing an optimised parameter set may be identified in the space defined by parameter values versus the likelihood function. A range is then defined within 1 % of the peak (for example, if the best-fit model has $r^2 = 0.500$ we report the range of parameters from models with $r^2 > 0.495$).

For each randomly selected set of parameter values (Table 1), the LEM computes a single time step, and the erosion in each grid cell is integrated. $E^*_{predicted}$ is then scaled by employing a log-transformation on all modelled catchments:

$$\log\left(K^*\right)=\frac{1}{N}\sum\left(\log\left(\frac{E_{predicted}}{K}\right)-\log\left(E_{apparent}\right)\right), \qquad (4)$$

$$\log\left(E^*_{predicted}\right)=\log\left(\frac{E_{predicted}}{K}\right)+\log\left(K^*\right), \qquad (5)$$

where N is the number of observations. The performance of $log(E^*_{predicted})$ against $log(E_{apparent})$ is then calculated for each parameter set. This setup offers the advantage of limiting the number of parameters varied; it is not our

https://doi.org/10.5194/esurf-2022-54
Preprint. Discussion started: 8 November 2022

aim to determine the absolute values of coefficients because these covary; instead, we focus on the ratio *D/K* (see Section 2.1).

After optimal values of A_c, *D/K* and/or *n* are found, the associated value of *K* can be corrected for log-transformation using an unbiased estimator (after Ferguson, 1989):

$$K = K^* e^{\frac{s^2}{2}}, \qquad (6)$$

where s^2 is an estimate of the variance:

$$s^2 = \frac{1}{N-1} \sum \left(\log\left(E_{apparent}\right) - \log\left(E^*_{predicted}\right) \right)^2, \qquad (7)$$

An equivalent form of Eqs 4–7 is used for the diffusion-only model, simply by replacing *K* with *D*. Although we believe this log transformation is justified, we show coefficients without Eqs 4–7 applied in Appendix C.

Given that our erosion rate data span several orders of magnitude, we compare log($E_{apparent}$) and log($E^*_{predicted}$) using the coefficient of determination (r^2) as implemented in the *scikit-learn Python* package (scikit-learn.org). This allows for direct comparison with previous studies that also use the r^2 metric in log-space to explore the controls on catchment-scale erosion rates (e.g., Portenga and Bierman, 2011; Harel et al., 2016). Optimised values are defined as the maximum r^2 value only if they are surrounded by local maxima in the likelihood, which is the case in all experiments below. Additionally, to gauge the sensitivity of results to the likelihood function, we provide results using Mean Absolute Error (MAE) for comparison in Appendix B.

2.3 The influence of lithology and precipitation on erosion

We subdivided the *OCTOPUS* catchments according to (1) areally-dominant lithology based on the GLiM global geologic map (Hartmann et al., 2012), which gives a vectorized description of lithology compiled from a number of regional high-resolution geologic maps at a target resolution of 1:1,000,000; and (2) spatially-averaged mean annual precipitation (MAP) using the WorldClim bioclimatic dataset (Hijmans et al., 2005).

Precipitation differences between lithologic subgroups can be significant; for instance, averages of 650 to 1390 mm for unconsolidated sediment and metamorphic rocks, respectively. To address lithological variation in the presence of climatic differences between lithologic subgroups in the advection-only model, we attempt to

https://doi.org/10.5194/esurf-2022-54
Preprint. Discussion started: 8 November 2022

isolate substrate effects with the form of the stream power equation given by Kooi and Beaumont (1996), which explicitly includes precipitation variations that are normally folded into K:

$$E_{predicted,advective} = K_{lith}(pA)^m S^n, \qquad (8)$$

Although many factors influence K besides precipitation, we use K_{lith} in this case to denote the variable we are attempting to isolate. We do not attempt to correct for variable precipitation in calculating D; for instance, by devising an equivalent D_{lith} from Eq. *8*.

3 Results

3.1 Advection-only model

We apply a stream power-based advection-only model (excluding hillslope diffusion), with two free parameters: a slope exponent (n) and critical drainage area (A_c). Variations in m are fixed to n such that concavity is held constant at m/n = 0.45. We report the optimised values in terms of maximum value and an optimised range of values that are within 1 % of the maximum (i.e., $Q_{0.01}$). The advection-only model (Fig. 2) is globally optimised at $n \sim 1.31$ ($Q_{0.01}$ = 1.17–1.33; Fig. 2a) and at $A_c \sim 0.06$ km^2 ($Q_{0.01}$ = 0.03–0.07 km^2; Fig. 2b). We note that these values do not change substantially when using the higher-resolution 1-arc-sec DEMs (Appendix A, Fig. A1). Optimal n increases to 1.47 ($Q_{0.01}$ = 1.23–1.61), while optimal A_c decreases to 0.02 km^2 ($Q_{0.01}$ = 0.01–0.04 km^2). The differences in n are likely the result of the sensitivity to higher catchment-averaged slopes in the 1-arc-sec DEMs (see supplementary Table S1). Additionally, both the 3-arc-sec and 1-arc-sec models show a consistent pattern of significant drop-off in r^2 values at 0.05–0.08 km^2, putting at least an upper limit on the optimal parameter value.

3.2 Diffusion-only model

The diffusion-only model (Fig. 3) is globally optimised with the hillslope diffusion constant, $p \sim 2.0$ (r^2 = 0.50, Fig. 3b). We find negligible dependence on DEM-resolution; $p \sim 2.0$ for the 1-arc-sec models (Appendix A, Figure A2).

https://doi.org/10.5194/esurf-2022-54
Preprint. Discussion started: 8 November 2022

3.3 Advection-diffusion model

While the optimisation of our diffusion-only model (Fig. 3) with $p = 2$ is an intriguing result that invites further investigation (cf. Gabet et al., 2021), we retain linear diffusion ($p = 1$) in our advection-diffusion experiment because for $p \neq 1$ the model is (1) numerically unstable when implemented in LEMs, and (2) it fails to accommodate hillslope deposition (i.e., does not conserve mass).

The advection-diffusion model (Fig. 4) is globally optimised at $n \sim 2.02$ ($Q_{0.01} = 1.51$–2.57; Fig. 4c), and $D/K \sim 4.56 \times 10^5\ m^{0.9n+1}$ ($Q_{0.01} = 9.01 \times 10^3 - 1.94 \times 10^7$; Fig. 4d). For n and D/K, the $Q_{0.01}$ ranges are quite broad in part because both parameters are co-dependent (Fig. 4a). Optimum $A_c \sim 0.04$ km^2 ($Q_{0.01} = 0.02$–0.37; Fig 4e) is similar to that from the advection-only models. The models are more diffusive when n is low and D/K is high, and $E_{predicted}$ is dependent mainly on catchment slope. This results in values clustering at $r^2 \sim 0.35$ (Fig. 4c, d, e) for models with high diffusion. Because D/K covaries with n (and m, Fig. 4a), we find that sediment transport derived from diffusional processes is maximised when $E_{predicted,diffusive}/E_{total}$ is ~ 0.39 (Fig. 4f).

4 Discussion

In their benchmark study, Portenga and Bierman (2011) employ stepwise regression to relate their compilation of ^{10}Be-derived erosion rates to a range of factors embracing topography, climate, lithology and seismicity. That study, along with the later inclusion of normalised steepness (e.g., Harel et al., 2016), added substantially to our knowledge of how and why erosion rate varies. Our alternative approach here focuses upon the erosional processes at play in terms of advective and diffusive mass flux, rather than attempting to interpret the machinations of landscape response to internal and external agents. A significant advantage is that relations between topography, erosion, and LEM parameters are derived at the scale of the DEM grid cell within each catchment, and success is gauged from the absolute difference between modelled ($E^*_{predicted}$) and ^{10}Be-derived ($E_{apparent}$) erosion rates—in other words, we evaluate LEM parameters as they are commonly implemented in the models.

4.1 Optimised parameters for landscape evolution models

We first consider some comparisons with previous work regarding advection-only approaches. Our optimised $A_c \sim 0.06$ km^2 (Fig. 2b) for the 3-arc-sec resolution models falls near the minimum of the range applied in previous studies, such as Whipple and Tucker (1999), who suggest 0.059–0.14 km^2. Our optimised $n \sim 1.3$ ($n \sim 1.47$ for the 1-arc-sec models) is much lower than the 2.6 reported by Harel et al. (2016), which is derived from regression of erosion rate and normalised steepness ($k_{s\ ref}$). Harel et al. (2016) then use the product of $k_{s\ ref}$ and a

https://doi.org/10.5194/esurf-2022-54
Preprint. Discussion started: 8 November 2022

Earth Surface Dynamics
Discussions
Open Access
EGU

scaling drainage area to calculate M_χ. In principle, M_χ and n should be similar to our K and n values; however, M_χ is integrated across the catchment, thus limiting the ability of these regressions to capture the inherent nonlinearity at the sub-catchment or sub-reach scale when $n \neq 1$. The large discrepancy between our globally optimised values of n and those of Harel et al. (2016) likely arises from this integration across the catchment or reach scale, whereas here we compute erosion rates at each DEM grid cell, allowing us to better capture the nonlinear effects of stream power on erosion when $n \neq 1$. Spatial heterogeneity in erosion rate is often controlled by steep areas in the catchment, such as knickpoints, and higher values of n amplify the proportion of erosion derived from steep areas relative to the rest of the catchment (Fig. 1).

While linear diffusion ($p = 1$) is commonly applied in landscape evolution studies (e.g., Braun and Willett, 2013), our optimised $p \sim 2$ for the diffusion-only model is consistent with Gabet al. (2021) in which erosion rate correlates best with the square of hillslope convexity. In response to Gabet et al. (2021), Struble and Roering (2021) point to a systematic underestimation of curvature in natural landscapes that may be an artefact of the numerical methods used for estimating curvature from DEMs. Gabet et al. (2021) employ high-resolution (~1 m) LIDAR data, but the broader point made by Struble and Roering (2021) poses a serious limitation for large-scale LEM analyses that are typically restricted to lower-resolution DEMs. In such cases, the need for mass conservation and numerical stability are important considerations. And yet, a diffusion equation with exponent $p \neq 1$ is numerically unstable, physically unexplained, and does not accommodate deposition (the result of negative curvature). What does it say about the utility of running LEMs on natural landscapes if the optimised parameter value ($p \sim 2$) cannot be implemented? Struble and Roering (2021) suggest that $p \sim 2$ enhances the influence of steep, rapidly eroding areas on average curvature, which are commonly underestimated by many methods. Below, we discuss how the influence of these steep areas may be approximated by the stream power equation coupled with linear diffusion.

Our advection-diffusion model allows us to explore aspects of how hillslope and river processes govern sediment flux in river catchments. Theoretically, for a catchment in a perfect state of mass-flux equilibrium (or steady state), hillslopes and rivers are eroding at the same rate, so either one should be equally useful as a proxy for erosion rate. There would be no apparent advantage to combining advection and diffusion in the same model since they would both yield the same average erosion rate. Landscapes are, however, more often not at steady state (at least over timescales integrated by cosmogenic ^{10}Be) and the slight dominance of advective erosion in our optimised model ($E_{predicted,diffusive}/E_{total} = 0.39$, in Fig. 4f) suggests that transient signals disproportionately affect catchment-averaged erosion rates.

https://doi.org/10.5194/esurf-2022-54
Preprint. Discussion started: 8 November 2022

The positive relationship we observe between optimised n and relative diffusivity gives rise to a compelling possibility: as diffusivity increases, advective erosion becomes less important as a proxy for the total average erosion rate within the catchment, and more of a proxy for transience focused at the most rapidly eroding zones. However, in the absence of diffusion, river incision must account for all sediment that would be otherwise eroded diffusively from hillslopes. The increase in optimised n with diffusivity therefore represents the expanding role of steep transient zones in dictating the catchment-scale erosion rate.

Our optimised result for the advection-diffusion model, $n \sim 2.02$ (Fig. 4b), is compatible with previous work suggesting that typically $n > 1$ (e.g., Lague, 2014; Harel et al., 2016). A value of $n \sim 2.02$ also has implications for the erosional response to climate change. When precipitation is included explicitly in the formulation (Eq. *8*), erosion scales nearly linearly with changes in mean annual precipitation (assuming m/n = 0.45). We return to this point in Section 4.2 below.

The best correlation between predicted and apparent erosion rates occurs when $D/K \sim 4.56 \times 10^5$ (Fig. 4d). This outcome broadly agrees with other studies that use K values in the range $\sim 10^{-8}$ to 10^{-5} $\mathrm{m}^{(n-1)}\ \mathrm{yr}^{-1}$ and D values in the expected range noted by Fernandes and Dietrich (1997) of 4.4×10^{-4} to 3.6×10^{-2} $\mathrm{m}^2\ \mathrm{yr}^{-1}$. Whipple et al. (2017) reports an optimal D/K ratio of 5×10^2 from Himalayan catchments, although fixing $n = 1$ in their models is a limiting assumption because D/K covaries with n, as we show. The diffusion model employed here assumes that the long-term flux of hillslope material is similar to the amount transported in one time-step. In reality, the catchment may not be at steady state and the hillslope erosion rate may change notably so as to change the rate of hillslope flux within individual catchments.

4.2 Erosion and precipitation

Correlating topographically-derived metrics with mean annual precipitation (MAP) on a global scale has been a long-standing goal. Harel et al. (2016) examine correlations between stream-power variables and climate as defined by the Köppen-Geiger scheme. In general, they find that $k_{s\,ref}$ and temperature covary inversely: warm deserts yield the highest $k_{s\,ref}$, and polar regions lowest, on average, although they also emphasise the large uncertainties. Because our approach compares model results to erosion rates, rather than using regression, we can more directly correlate K as it is implemented in LEMs under differing precipitation regimes.

We calculate coefficients D (for diffusion-only) or K (for advection models) for each of the optimised models using Eq. (*5*) in catchments that correspond to 40 different MAP bins distributed such that each bin has an approximately equal number of data points (N = 91 ± 1; Fig. 5). By looking at how these coefficients vary

https://doi.org/10.5194/esurf-2022-54
Preprint. Discussion started: 8 November 2022

Earth Surface Dynamics Discussions
Open Access
EGU

within each bin, we effectively reduce the influence of topography and isolate the relationship between erosion rate and precipitation. For reference, we also show results which do not apply a log-transformation correction from Eq. *6*, in Appendix C.

Optimised coefficients show a local peak in erosion rates centred around 330 mm yr^{-1} and then dipping overall from around 1100 to 1600 mm yr^{-1} before increasing again for extremely wet regions (Fig. 5b). These results agree well with the classic work of Langbein and Schumm (1958), which suggests that the fastest eroding environments are semi-arid (~ 250 mm yr^{-1}). This relationship is thought to be a product of the interplay between erosion, vegetation, total precipitation, and storm frequency in semi-arid regions—an outcome reproduced by Istanbulluoglu and Bras (2006), who show a positive relationship between sediment transport and the effects of reduced sediment cover/increased runoff during drought.

While Langbein and Schumm (1958) had scant access to data from wetter settings, our results reveal an upward trend in coefficient values for MAP > 1500 mm yr^{-1} (Fig. 5). This is in line with Walling and Kleo's (1979) global study of sediment yield and climate, which also shows a further major peak at ~ 800 mm yr^{-1} attributed to the most expansive agricultural production globally (Hyman et al., 2016). In contrast to Walling and Kleo (1979), which does not isolate the effects of variable land use, topography, and geology on sediment yields, our use of long-term erosion rates means that we can largely ignore the effects of land use. This may explain the subdued peak ~ 800 mm yr^{-1} in our data. However, when no log transformation is applied to the coefficients, the peak at 800 mm yr^{-1} rises while the peak at 300 mm yr^{-1} is suppressed.

Marder and Gallen (2022) find a nonlinear relationship between ^{10}Be-derived erosion rate and k_{sn} via regression; they also find that n increases with increasing erosion rate. However, k_{sn} is calculated by integrating along different channel lengths (as with Harel et al., 2016), whereas we calculate erosion at every grid cell and so capture local variations in erosion rate more effectively. We envisage cases in which steep zones, such as knickpoints, are responsible for a large proportion of the total catchment erosional flux, even though they represent a small fraction of the drainage area (e.g., Willenbring et al., 2013). Where erosion is a nonlinear function of slope and drainage area, an average of these erosion rates is unlikely to be proportional to the integrated k_{sn}.

https://doi.org/10.5194/esurf-2022-54
Preprint. Discussion started: 8 November 2022

Earth Surface Dynamics Discussions

4.3 Erosion and lithology

The variability in LEM parameters within each lithological bin was assessed following a similar approach to Section 4.2, with the additional step of employing K_{lith} (Eq. *8*) to isolate the effects of lithology on K in the advection-only model in the face of variable precipitation within lithologic subgroups.

Our results are largely as expected: all three models agree on the general tendency of sedimentary rocks being most erodible and plutonic/volcanic being least, although the relative magnitudes of these differences vary between models. Unconsolidated sedimentary rock is the most erodible of all according to the diffusion and advection-only models (Fig. 6b). Models disagree about the least erodible subcategories: basic plutonic, intermediate volcanic, or pyroclastic. The pyroclastic and basic plutonic rock-types show the most variance. For pyroclastic, the advection models suggest relatively low erodibility, whereas the diffusion-only models suggest moderate erodibility.

We note that the three-fold range in erodibility (Fig. 6b) is much lower than that reported elsewhere, in some cases by several orders of magnitude (Sklar and Dietrich, 2001; Garcia-Castellanos et al., 2018). This may be due to the greater focus on the differential erodibility within individual sites (Garcia-Castellanos et al., 2018). Despite our efforts to account for some of the covarying with MAP, our analysis inevitably smooths out some variability owing to the diversity of catchments incorporated within each lithological bin. Moreover, erodibility is clearly a function of several additional factors such as fracture spacing (e.g., Neely et al., 2019), and weathering conditions, which is challenging to address in a global analysis such as ours.

5. Conclusions

We have examined the most widely used parameters applied to a set of three landscape evolution model set ups: (1) a stream-power based, advection-only model; (2) a diffusion-only model; and (3) an advection-diffusion hybrid model. We optimised the parameter values by comparing directly the catchment-averaged erosion rates predicted by our three models with a global catalogue of ^{10}Be-derived catchment-averaged erosion rates (Codilean et al., 2022).

The diffusion-only model outperformed the advection-only model when applying $p \sim 2$. However, the physical implications and numerical limitations of this result make it impractical for implementation in landscape evolution models. Instead, we propose that linear diffusion coupled with fluvial erosion (advection-diffusion) captures a high proportion of sediment derived from rapidly eroding, steep areas in a similar sense to a diffusion model with exponent $p \sim 2$. In the advection-diffusion hybrid model, the best agreement between the predicted and apparent erosion rates is observed with $n \sim 2.0$ (assuming a fixed concavity, $m/n = 0.45$), while the ratio of diffusivity/advection coefficient (D/K) is optimised at $\sim 4.56 \times 10^5$.

The Monte Carlo method employed here is a simple and powerful means of identifying ideal parameter sets over large spatial scales and is especially useful for dealing with sparse datasets. We applied the same approach to elucidate differences in optimal LEM parameters when considering lithology and precipitation. By looking at the LEM coefficients, we were able to better account for the influence of topography when isolating the relationship between erosion rate and precipitation/ lithology. Of particular interest was a general upward trend in the coefficients (K and D) with respect to precipitation, and a local maxima centred at ~300 mm/yr. This local maxima may represent the higher erodibility of semi-arid environments as identified by Langbein and Schumm (1958). Nevertheless, many other influences on erosion are yet to be explored in a satisfactory and robust way. Future studies may use these parameter ranges as a baseline to inform large landscape evolution studies. Moreover, our methodology could be extended to incorporate more complexity into the canonical advection and diffusion-based equations applied here.

Author contributions: GR conceived the study, performed data analysis, and devised the code. JDJ and PV assisted with framing the study, and LYM performed code analysis. All co-authors contributed significantly to MS production.

Resource availability: The functions and notebooks for running this analysis are available from www.github.com/ruetg/lem_global_optimize .

Acknowledgments: Many thanks to Bruce Wilkinson for his guidance in framing the study, and to Daniel Garcia-Castellanos and Kim Huppert for their constructive advice. Several calculations were performed on the CSDMS Blanca HPC at the University of Colorado, Boulder. Maps in Figure 1 were produced using PyGMT (pygmt.org) .

Competing Interest: Authors declare no competing interests

References

Adams, B.A., Whipple, K.X., Forte, A.M., Heimsath, A.M. and Hodges, K.V., 2020. Climate controls on erosion in tectonically active landscapes. Science advances, 6(42), p.eaaz3166.

Barnhart, K.R., Tucker, G.E., Doty, S.G., Shobe, C.M., Glade, R.C., Rossi, M.W. and Hill, M.C., 2020. Inverting topography for landscape evolution model process representation: 1. Conceptualization and sensitivity analysis. Journal of Geophysical Research: Earth Surface, 125(7), p.e2018JF004961.

Barnes, R., Lehman, C. and Mulla, D., 2014. Priority-flood: An optimal depression-filling and watershed-labeling algorithm for digital elevation models. *Computers & Geosciences*, *62*, pp.117-127.

Beven, K. and Binley, A., 1992. The future of distributed models: model calibration and uncertainty prediction. *Hydrological processes*, *6*(3), pp.279-298.

Beven, K. and Binley, A., 2014. GLUE: 20 years on. *Hydrological processes*, *28*(24), pp.5897-5918.

Brown, L.R., 1981, World population growth, soil erosion, and food security: Science, v. 214, p. 995–1002, doi: 10.1126/science.7302578

Carretier, S., Regard, V., Vassallo, R., Aguilar, G., Martinod, J., Riquelme, R., Christophoul, F., Charrier, R., Gayer, E., Farías, M. and Audin, L., 2015. Differences in 10Be concentrations between river sand, gravel and pebbles along the western side of the central Andes. *Quaternary Geochronology*, *27*, pp.33-51.

Codilean, A.T., Munack, H., Saktura, W.M., Cohen, T.J., Jacobs, Z., Ulm, S., Hesse, P.P., Heyman, J., Peters, K.J., Williams, A.N. and Saktura, R.B., 2022. *OCTOPUS* database (v. 2). *Earth System Science Data*, *14*(8), pp.3695-3713.

Croissant, T., and Braun, J. (2014). Constraining the stream power law: a novel approach combining a landscape evolution model and an inversion method. *Earth surface dynamics*, *2*(1), 155-166.

Csilléry, K., Blum, M.G., Gaggiotti, O.E. and François, O., 2010. Approximate Bayesian computation (ABC) in practice. *Trends in ecology & evolution*, *25*(7), pp.410-418.

Fernandes, N.F., Dietrich, W.E., 1997. Hillslope evolution by diffusive processes: The timescale for equilibrium adjustments. *Water Resources Research*, *33*(6), pp.1307-1318.

https://doi.org/10.5194/esurf-2022-54
Preprint. Discussion started: 8 November 2022

Fontana, G. D., & Marchi, L. (2003). Slope–area relationships and sediment dynamics in two alpine streams. *Hydrological Processes*, *17*(1), 73-87.

Forte, A.M., Whipple, K.X., Bookhagen, B. and Rossi, M.W., 2016. Decoupling of modern shortening rates, climate, and topography in the Caucasus. *Earth and Planetary Science Letters*, *449*, pp.282-294.

Fox, M., Goren, L., May, D.A. and Willett, S.D., 2014. Inversion of fluvial channels for paleorock uplift rates in Taiwan. *Journal of Geophysical Research: Earth Surface*, *119*(9), pp.1853-1875.

Gabet, E.J., Mudd, S.M., Wood, R.W., Grieve, S.W.D., Binnie, S.A. and Dunai, T.J., 2021. Hilltop Curvature Increases with the Square Root of Erosion Rate. *Journal of Geophysical Research: Earth Surface*, *126*(5), p.e2020JF005858.

Garcia-Castellanos, D., Vergés, J., Gaspar Escribano, J. and Cloetingh, S., 2003. Interplay between tectonics, climate, and fluvial transport during the Cenozoic evolution of the Ebro Basin (NE Iberia). *Journal of Geophysical Research: Solid Earth*, *108*(B7).

Garcia-Castellanos, D. and O'Connor, J.E., 2018. Outburst floods provide erodability estimates consistent with long-term landscape evolution. *Scientific Reports*, *8*(1), pp.1-9.

Gallen, S.F., Wegmann, K.W. and Bohnenstiehl, D.R., 2013. Miocene rejuvenation of topographic relief in the southern Appalachians. *GSA Today*, *23*(2), pp.4-10.

Gailleton, B., Mudd, S. M., Clubb, F. J., Grieve, S. W., & Hurst, M. D. (2021). Impact of changing concavity indices on channel steepness and divide migration metrics. *Journal of Geophysical Research: Earth Surface*, *126*(10), e2020JF006060.

Gesch, D., Oimoen, M., Greenlee, S., Nelson, C., Steuck, M. and Tyler, D., 2002. The national elevation dataset. *Photogrammetric engineering and remote sensing*, *68*(1), pp.5-32.

Granger, D.E., Kirchner, J.W., and Finkel, R., 1996. Spatially averaged long-term erosion rates measured from in-situ produced cosmogenic nuclides in alluvial sediment Journal of Geology, 104, pp. 249-257.

Harel, M.A., Mudd, S.M. and Attal, M., 2016. Global analysis of the stream power law parameters based on worldwide 10Be denudation rates. Geomorphology, 268, pp.184-196.

Hartmann, J. and Moosdorf, N., 2012. The new global lithological map database GLiM: A representation of rock properties at the Earth surface. *Geochemistry, Geophysics, Geosystems*, *13*(12).

Hijmans, R.J., Cameron, S.E., Parra, J.L., Jones, P.G. and Jarvis, A., 2005. Very high resolution interpolated climate surfaces for global land areas. *International Journal of Climatology: A Journal of the Royal Meteorological Society*, *25*(15), pp.1965-1978.

https://doi.org/10.5194/esurf-2022-54
Preprint. Discussion started: 8 November 2022

Hooke, R. LeB., 2000. On the history of humans as geomorphic agents. Geology 28 (9): 843–846.

Howard, A.D., Dietrich, W.E. and Seidl, M.A., 1994. Modeling fluvial erosion on regional to continental scales. *Journal of Geophysical Research: Solid Earth*, 99(B7), pp.13971-13986.

Hyman, G., Barona, E., Biradar, C., Guevara, E., Dixon, J., Beebe, S., Castano, S.E., Alabi, T., Gumma, M.K., Sivasankar, S. and Rivera, O., 2016. Priority regions for research on dryland cereals and legumes. *F1000Research*, *5*.

Istanbulluoglu, E., Bras, R.L., 2006. On the dynamics of soil moisture, vegetation, and erosion: Implications of climate variability and change. *Water Resources Research 42*(6).

Kooi, H. and Beaumont, C., 1996. Large-scale geomorphology: Classical concepts reconciled and integrated with contemporary ideas via a surface processes model. *Journal of Geophysical Research: Solid Earth*, *101*(B2), pp.3361-3386.

Lague, D., & Davy, P. (2003). Constraints on the long-term colluvial erosion law by analyzing slope□area relationships at various tectonic uplift rates in the Siwaliks Hills (Nepal). *Journal of Geophysical Research: Solid Earth*, *108*(B2).

Lague, D., 2014. The stream power river incision model: evidence, theory and beyond. *Earth Surface Processes and Landforms*, *39*(1), pp.38-61.

Langbein, W.B. and Schumm, S.A., 1958. Yield of sediment in relation to mean annual precipitation. *Eos, Transactions American Geophysical Union*, *39*(6), pp.1076-1084.

Lehner, B., Verdin, K. and Jarvis, A., 2008. New global hydrography derived from spaceborne elevation data. *Eos, Transactions American Geophysical Union*, *89*(10), pp.93-94.

Lukens, C. E., Riebe, C. S., Sklar, L. S., & Shuster, D. L. (2016). Grain size bias in cosmogenic nuclide studies of stream sediment in steep terrain. *Journal of Geophysical Research: Earth Surface*, 121(5), 978-999.

Lal, D., 1991. Cosmic ray labeling of erosion surfaces: in situ nuclide production rates and erosion models. *Earth and Planetary Science Letters*, *104*(2-4), pp.424-439.

Marder, E. and Gallen, S.F., 2022. Climate controls on fluvial topography. *Journal of Geophysical Research: Solid Earth*, 104, pp.28957-28981.

Miller, S.R., Sak, P.B., Kirby, E. and Bierman, P.R., 2013. Neogene rejuvenation of central Appalachian topography: Evidence for differential rock uplift from stream profiles and erosion rates. *Earth and Planetary Science Letters*, *369*, pp.1-12.

https://doi.org/10.5194/esurf-2022-54
Preprint. Discussion started: 8 November 2022

Mudd, S. M. (2016). Detection of transience in eroding landscapes. *Earth Surface Processes and Landforms*, 42(1), 24-41.

Neely et al. 2019. Bedrock fracture density controls on hillslope erodibility in steep, rocky landscapes with patchy soil cover, southern California, USA. *Earth and Planetary Science Letters*, 522, 186-197.

Pedersen, V.K., Braun, J. and Huismans, R.S., 2018. Eocene to mid-Pliocene landscape evolution in Scandinavia inferred from offshore sediment volumes and pre-glacial topography using inverse modelling. *Geomorphology*, *303*, pp.467-485.

Perron, J.T., Dietrich, W.E. and Kirchner, J.W., 2008. Controls on the spacing of first-order valleys. *Journal of Geophysical Research: Earth Surface*, *113*(F4).

Pico, T., Mitrovica, J.X., Perron, J.T., Ferrier, K.L. and Braun, J., 2019. Influence of glacial isostatic adjustment on river evolution along the US mid-Atlantic coast. *Earth and Planetary Science Letters*, *522*, pp.176-185.

Portenga, E.W., Bierman, P.R. and Reusserm L., 2011, Understanding Earth's eroding surface with ^{10}Be: *GSA Today*, 21, pp. 4-10.

Riebe, C. S., Sklar, L. S., Lukens, C. E., & Shuster, D. L. (2015). Climate and topography control the size and flux of sediment produced on steep mountain slopes. *Proceedings of the National Academy of Sciences*, 112(51), 15574-15579.

Roering, J.J., Perron, J.T. and Kirchner, J.W., 2007. Functional relationships between denudation and hillslope form and relief. *Earth and Planetary Science Letters*, *264*(1-2), pp.245-258.

Ruetenik, G., Moucha, R. and de Boer, B., 2019. Deformation in response to landscape evolution during glacial cycles on the US Atlantic passive margin. *Earth and Planetary Science Letters*, *526*, p.115759.

Simoes, M., Braun, J. and Bonnet, S., 2010. Continental-scale erosion and transport laws: A new approach to quantitatively investigate macroscale landscapes and associated sediment fluxes over the geological past. *Geochemistry, Geophysics, Geosystems*, *11*(9).

Sklar, L., and Dietrich, W.E. 2001. Sediment supply, grain size and rock strength controls on rates of river incision into bedrock. *Geology*, 29:1087–1090.

Starke, J., Ehlers, T.A., Schaller, M., 2020. Latitudinal effect of vegetation on erosion rates identified along western South America. *Science,* 367, 1358-1361.

Struble, W.T. and Roering, J.J., 2021. Hilltop curvature as a proxy for erosion rate: Wavelets enable rapid computation and reveal systematic underestimation. *Earth Surface Dynamics Discussions*, pp.1-35.

Temme, A.J.A.M., Baartman, J.E.M. and Schoorl, J.M., 2009. Can uncertain landscape evolution models discriminate between landscape responses to stable and changing future climate? A millennial-scale test. *Global and Planetary Change*, *69*(1-2), pp.48-58.

Theodoratos, N., Seybold, H. and Kirchner, J.W., 2018. Scaling and similarity of a stream-power incision and linear diffusion landscape evolution model. *Earth Surface Dynamics*, *6*(3), pp.779-808.

Von Blanckenburg, F. (2005). The control mechanisms of erosion and weathering at basin scale from cosmogenic nuclides in river sediment. *Earth and Planetary Science Letters*, 237(3-4), 462-479.

Walling, D.E., Kleo, A.H.A., 1979. Sediment yields of rivers in areas of low precipitation: a global view. *Proceedings... The Hydrology of areas of low precipitation*.

Willenbring, J. K., Gasparini, N. M., Crosby, B. T., & Brocard, G., 2013b. What does a mean mean? The temporal evolution of detrital cosmogenic denudation rates in a transient landscape. *Geology*, 41(12), 1215-1218.

Whipple, K.X. and Tucker, G.E., 1999. Dynamics of the stream□power river incision model: Implications for height limits of mountain ranges, landscape response timescales, and research needs. *Journal of Geophysical Research: Solid Earth*, 104(B8), pp.17661-17674.

Whipple, K.X., Forte, A.M., DiBiase, R.A., Gasparini, N.M. and Ouimet, W.B., 2017. Timescales of landscape response to divide migration and drainage capture: Implications for the role of divide mobility in landscape evolution. *Journal of Geophysical Research: Earth Surface*, *122*(1), pp.248-273.

Wobus, C., Whipple, K.X., Kirby, E., Snyder, N., Johnson, J., Spyropolou, K., Crosby, B., Sheehan, D. and Willett, S.D., 2006. Tectonics from topography: Procedures, promise, and pitfalls. *Special papers, Geological Society of America*, 398, p.55.

Zavala, V., Carretier, S., & Bonnet, S. (2020). Influence of orographic precipitation on the topographic and erosional evolution of mountain ranges. *Basin Research*, 32(6), 1574-1599.

https://doi.org/10.5194/esurf-2022-54
Preprint. Discussion started: 8 November 2022

Earth Surface Dynamics Discussions Open Access EGU

580

Tables and Figures

Table 1: Parameter values and ranges for the three model set ups.

Model set	Parameter	Range	Sampling
Stream power only	n	0–4	Random, 1000 samples
	A_c	0.01–8 km^2	Random, log-uniform, 1000 samples
Diffusion only	p	0–4	Linear increment by 0.2
Stream power + diffusion	n	0–4	Random, 10,000 samples
	D/K	10^2–10^9 $m^{0.9n+1}$	Random, log-uniform, 10,000 samples
	A_c	0.01–8 km^2	Random, log-uniform, 10,000 samples

https://doi.org/10.5194/esurf-2022-54
Preprint. Discussion started: 8 November 2022

Earth Surface Dynamics Discussions Open Access EGU

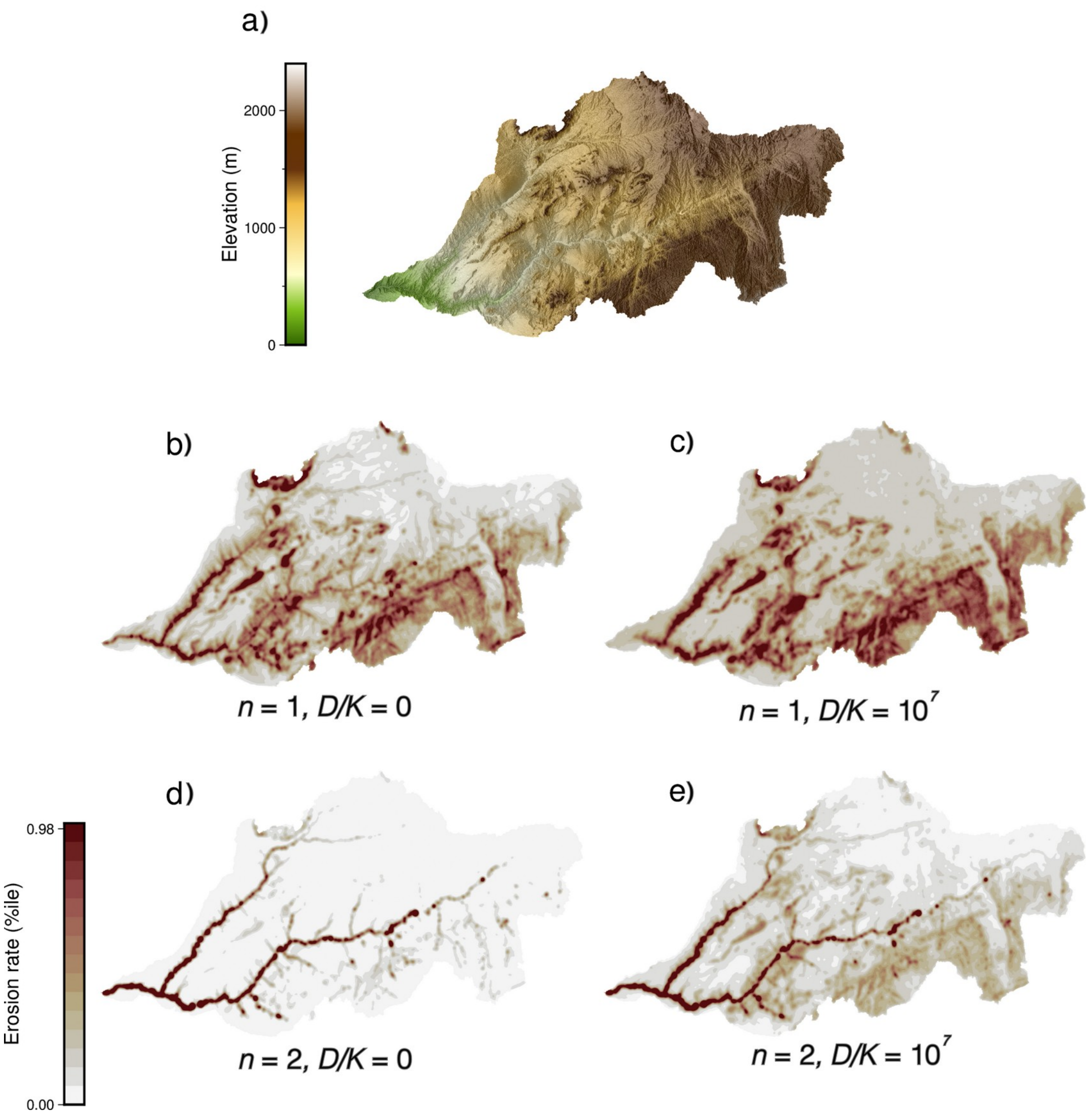

585 **Figure 1:** a) Catchment example (Swakop River, Namibia) clipped from a *Hydrosheds* DEM based on the shapefile provided in *OCTOPUS* v.2. Lower panels show corresponding relative erosion rates (colour ramp spans 0–98 % of the range) for different parameter values. No diffusion is included in (b) and (d), hence erosion is focused in the channels. In (c) and (e), a moderately high (10^7) diffusivity is used relative to advection, which causes erosion to be more focused on hillslopes.

https://doi.org/10.5194/esurf-2022-54
Preprint. Discussion started: 8 November 2022

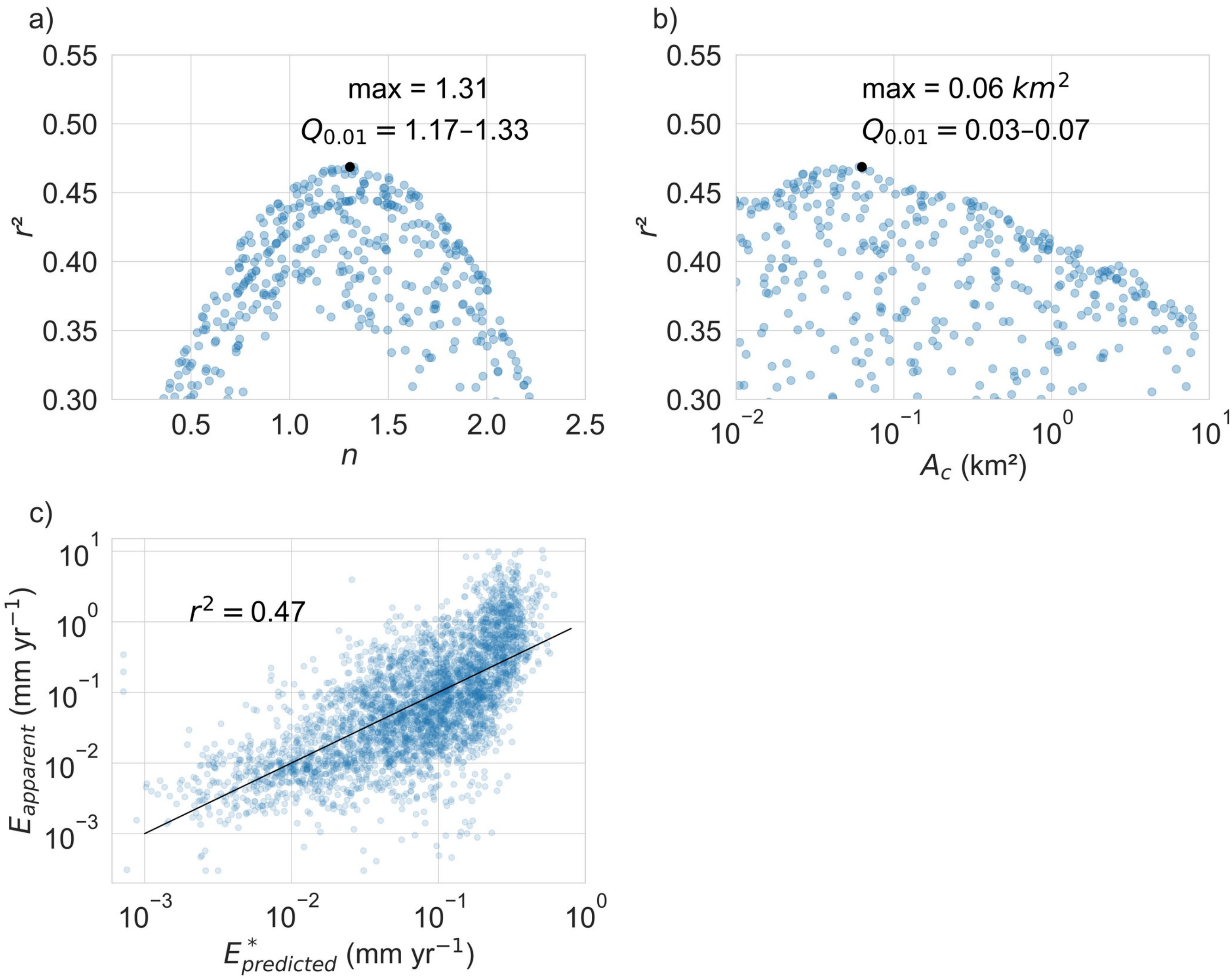

Figure 2: The advection-only model. a) optimised $n = 1.31$ ($Q_{0.01} = 1.17$–1.33), with a global maximum of 1.31, b) optimised $A_c = 0.06$ km^2 ($Q_{0.01} = 0.03$–0.07 km^2), c) apparent vs predicted erosion rate yields $r^2 = 0.47$; no regression is performed, the black line indicates a perfect 1:1 fit.

https://doi.org/10.5194/esurf-2022-54
Preprint. Discussion started: 8 November 2022

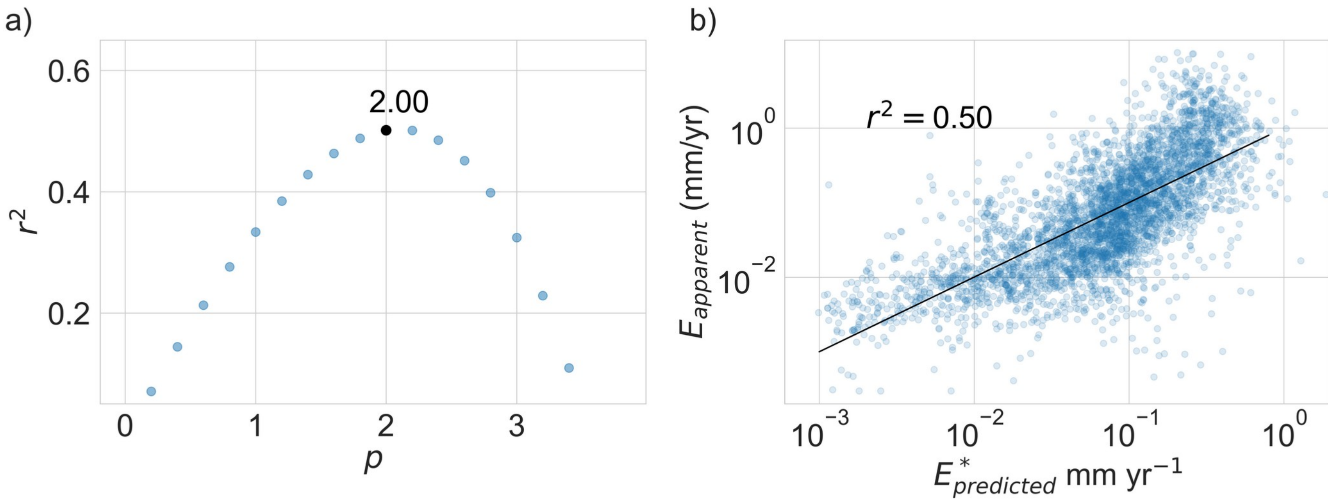

Figure 3: The diffusion-only model. a) the sole free parameter (p) is optimised at p = 2.00. b) Apparent vs predicted erosion rate yields r^2 = 0.50; no regression is performed, the black line indicates a perfect 1:1 fit.

https://doi.org/10.5194/esurf-2022-54
Preprint. Discussion started: 8 November 2022

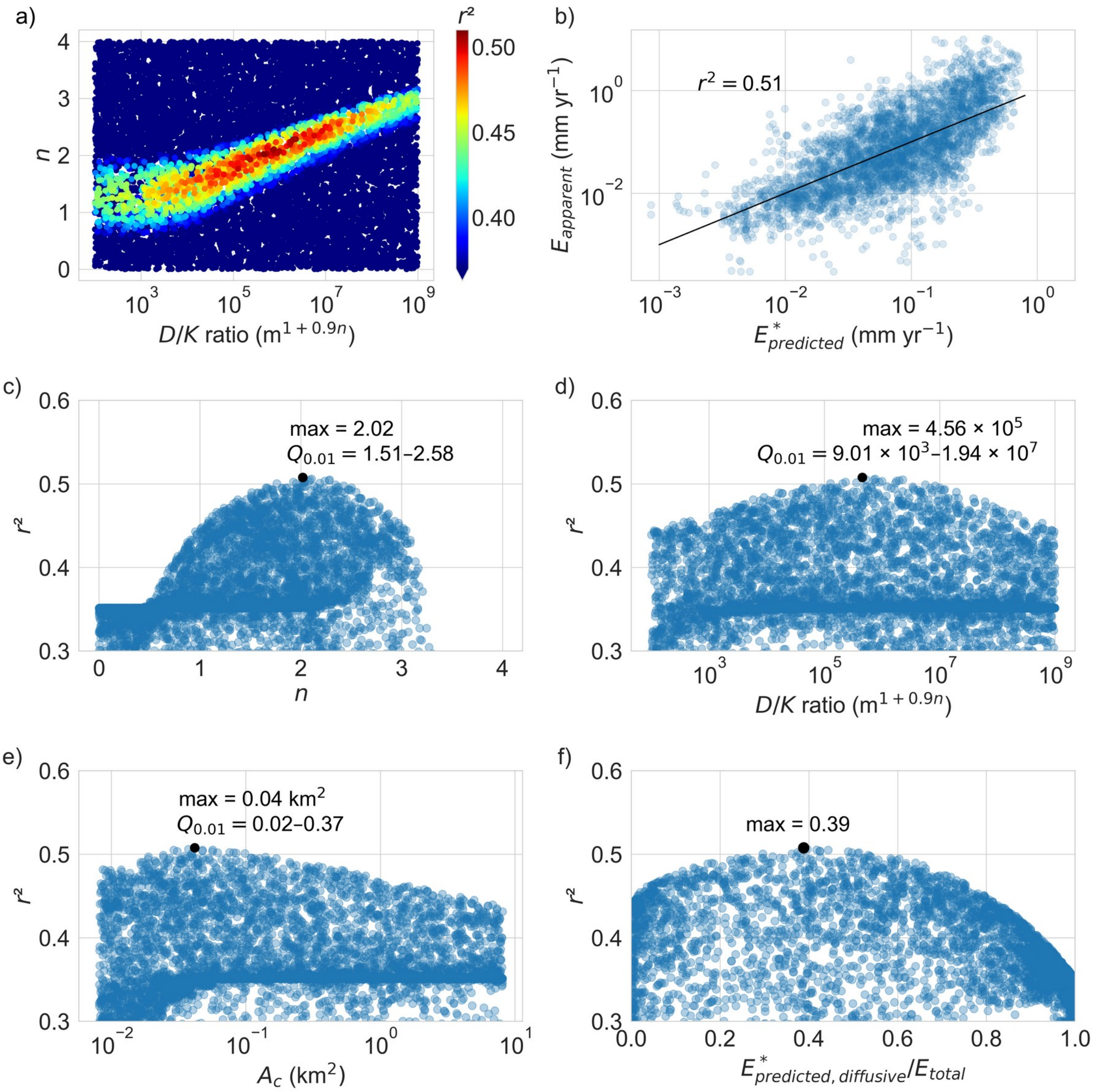

Figure 4: Model parameters representing variations in the relative dominance of advection vs diffusion. a) Covariance of *D/K* with *n*; when *D/K* is low (no diffusion), optimal *n* approaches ~1.3 (y intercept). b) The best correspondence between $E^*_{predicted}$ and $E_{apparent}$ is achieved with $r^2 = 0.51$, where c) $n \sim 2.02$ ($Q_{0.01}$ = 1.51–2.57); d) $D/K \sim 4.56 \times 10^5$ ($Q_{0.01} = 9.01 \times 10^3$–$1.94 \times 10^7$), albeit with a fairly broad peak, and e) $A_c \sim 0.04$ km^2 ($Q_{0.01}$ = 0.02–0.37 km^2). Clustering at $r^2 \sim 0.35$ in panels (c, d, e) represents parameter sets where diffusion dominates over advection. f) Sediment transport derived from diffusional processes is maximised when $E_{predicted,diffusive}/E_{total}$ is ~ 0.39.

25

https://doi.org/10.5194/esurf-2022-54
Preprint. Discussion started: 8 November 2022

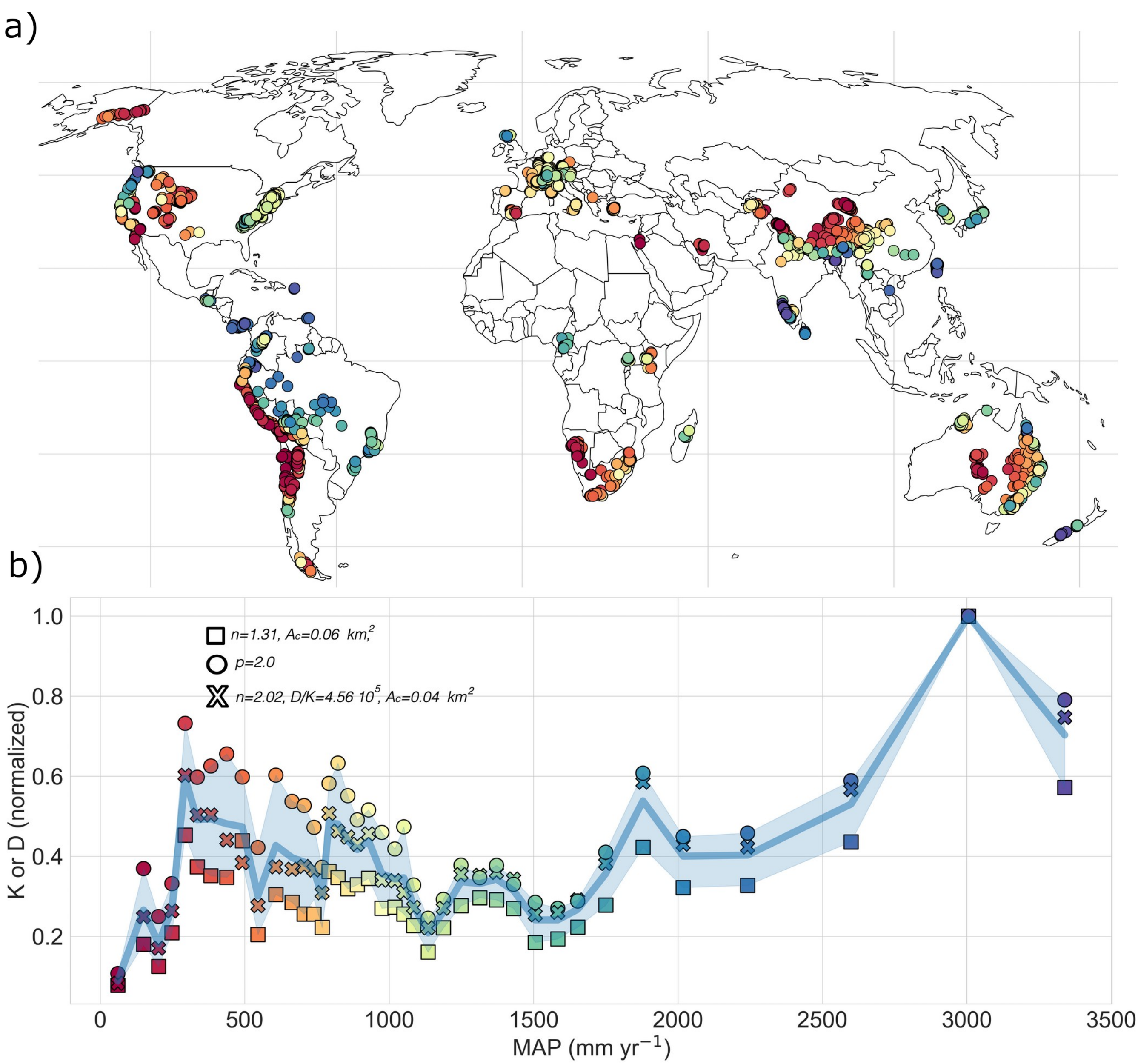

Figure 5: a) Global distribution of catchments in the *OCTOPUS* v.2 (Codilean et al., 2022) catalogue of erosion
610 rates coloured by mean annual precipitation (MAP). b) Coefficients for diffusion (circle), advection (square), and advection-diffusion (X) calculated for each globally optimised model per MAP bin. Both panels use the same colour ramp, which corresponds to the MAP bin; blue shading represents the range spanned by the 3 models, and heavy blue-line is the mean.

https://doi.org/10.5194/esurf-2022-54
Preprint. Discussion started: 8 November 2022

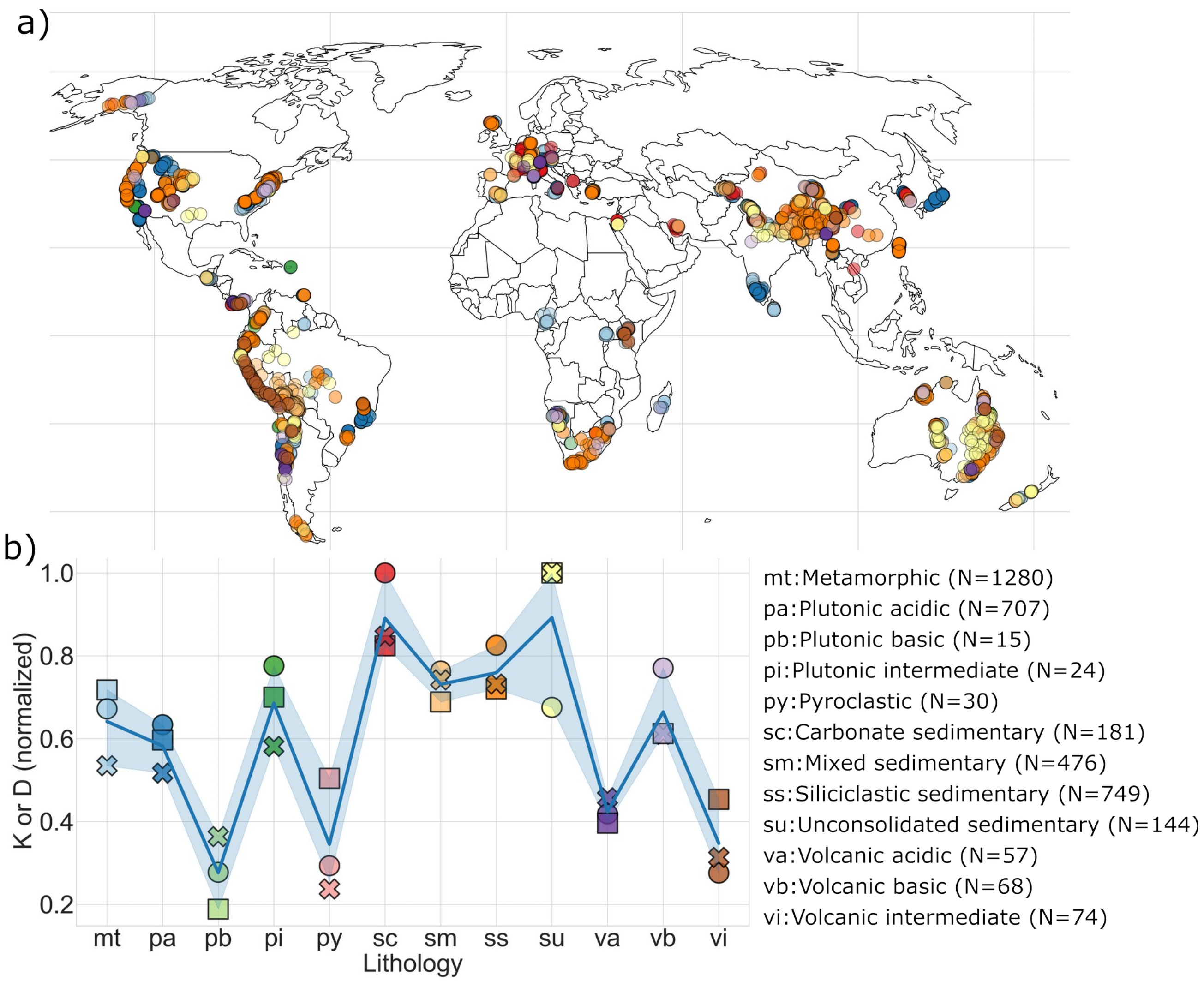

Figure 6: a) Global distribution of catchments in the *OCTOPUS* v.2 catalogue (Codilean et al., 2022) of erosion rates coloured by dominant lithology. b) Coefficients (normalised by their maximum values) for different best-fit models within twelve lithologic subsets from Hartmann et al. (2012). Coefficients for diffusion (x), advection (square), and advection-diffusion (circle) calculated for each globally optimised model per lithologic bin; blue shading represents the range spanned by the 3 models, and heavy blue-line is the mean. Both panels use the same colour ramp, which corresponds to the lithologic bin.

https://doi.org/10.5194/esurf-2022-54
Preprint. Discussion started: 8 November 2022

Earth Surface Dynamics
Discussions
Open Access

Appendix A: High-resolution (1-arc-sec DEM) model results

Results of advection-only and diffusion-only models run with 1-arc-sec resolution of the *OCTOPUS* catchments with fewer than 1.3×10^{7} DEM cells (1 square degree) in area (N = 3414). The results are largely consistent with those run with the 3-arc-sec DEM (Figs. 2 and 3). Much of the difference in n may be attributed to the higher average slopes from the higher-resolution 1-arc-sec model (see supplementary Table 1*)*. The differences in the upper limits of the drainage area are consistent in that both 3-arc-sec and 1-arc-sec resolution models show steep drop-off in r^2 at 0.05–0.08 km^2.

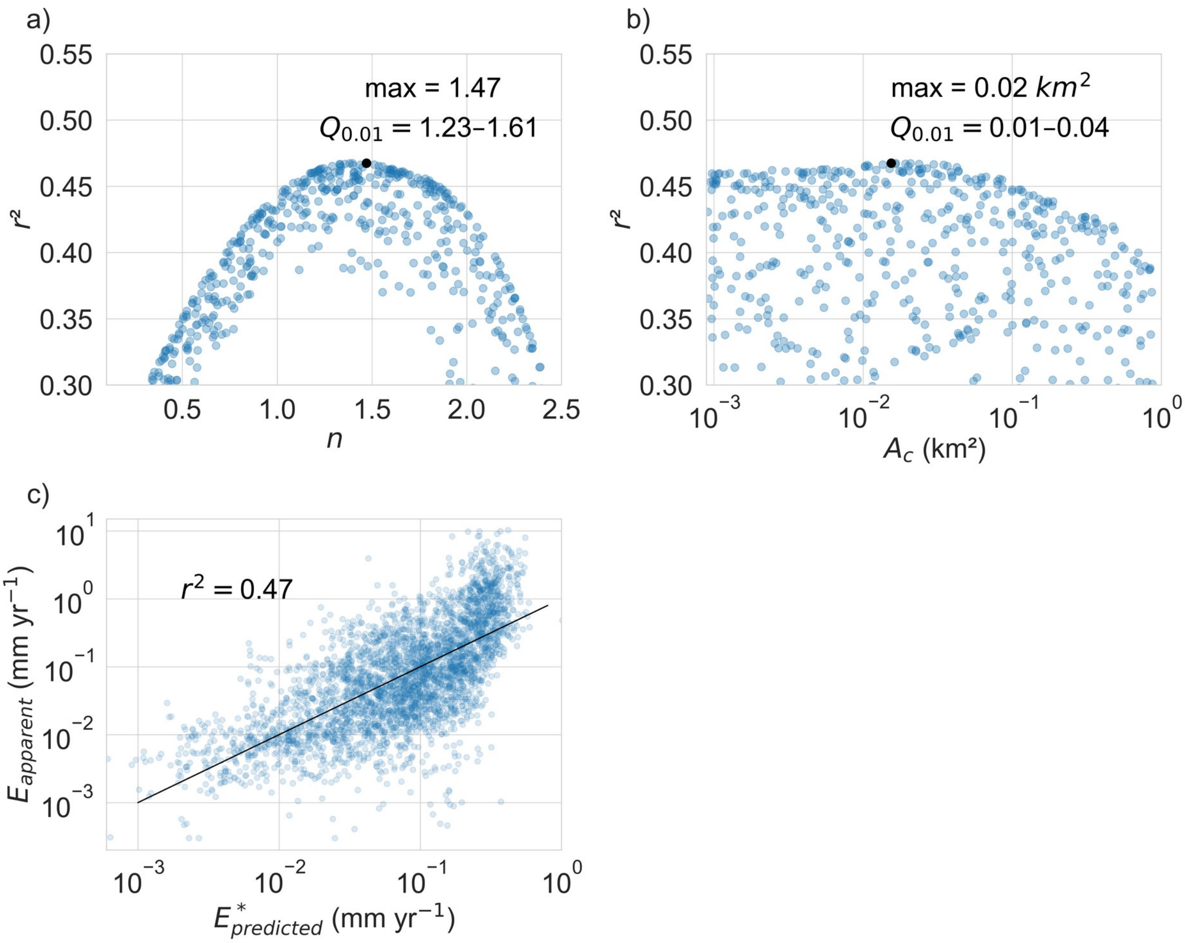

Figure A1: The advection-only model with 1-arc-sec DEM. a) Optimal n = 1.47 ($Q_{0.01}$ = 1.23–1.61), which is slightly higher relative to the 3-arc-sec resolution model. b) Optimal A_c = 0.02 km^2 ($Q_{0.01}$ = 0.01–0.04 km^2), which is slightly lower relative to the low-resolution model. Note however, the similar r^2 of 0.47 (c).

https://doi.org/10.5194/esurf-2022-54
Preprint. Discussion started: 8 November 2022

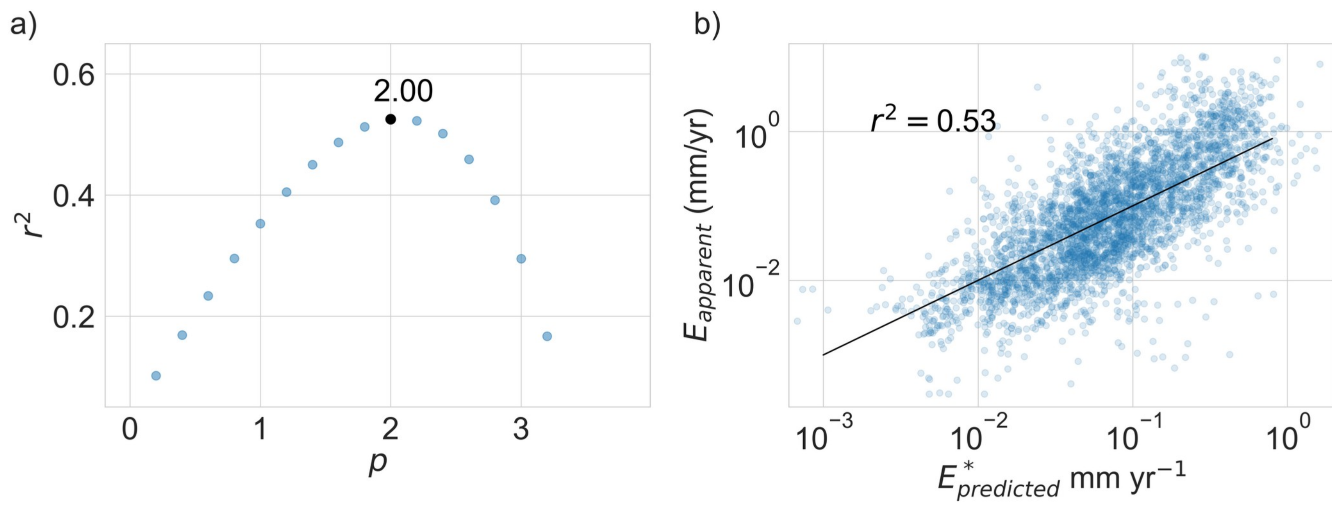

Figure A2: The diffusion-only model 1-arc-sec DEM. a) Optimal $p = 2.0$ is consistent with that of the lower resolution model and gives a similar $r^2 = 0.53$ (b).

https://doi.org/10.5194/esurf-2022-54
Preprint. Discussion started: 8 November 2022

Appendix B: Supplemental likelihood function results

When using Mean absolute error as the likelihood function for the 3-arc-sec resolution models, the best-fit estimates are largely similar to the results using r^2. However, MAE is meaningful for those looking for the quality of the fit in more absolute terms. The best-fit models have MAE < 0.45 error in logged erosion rates (in mm yr^{-1}), which is notable given the high variability of catchments we are dealing with.

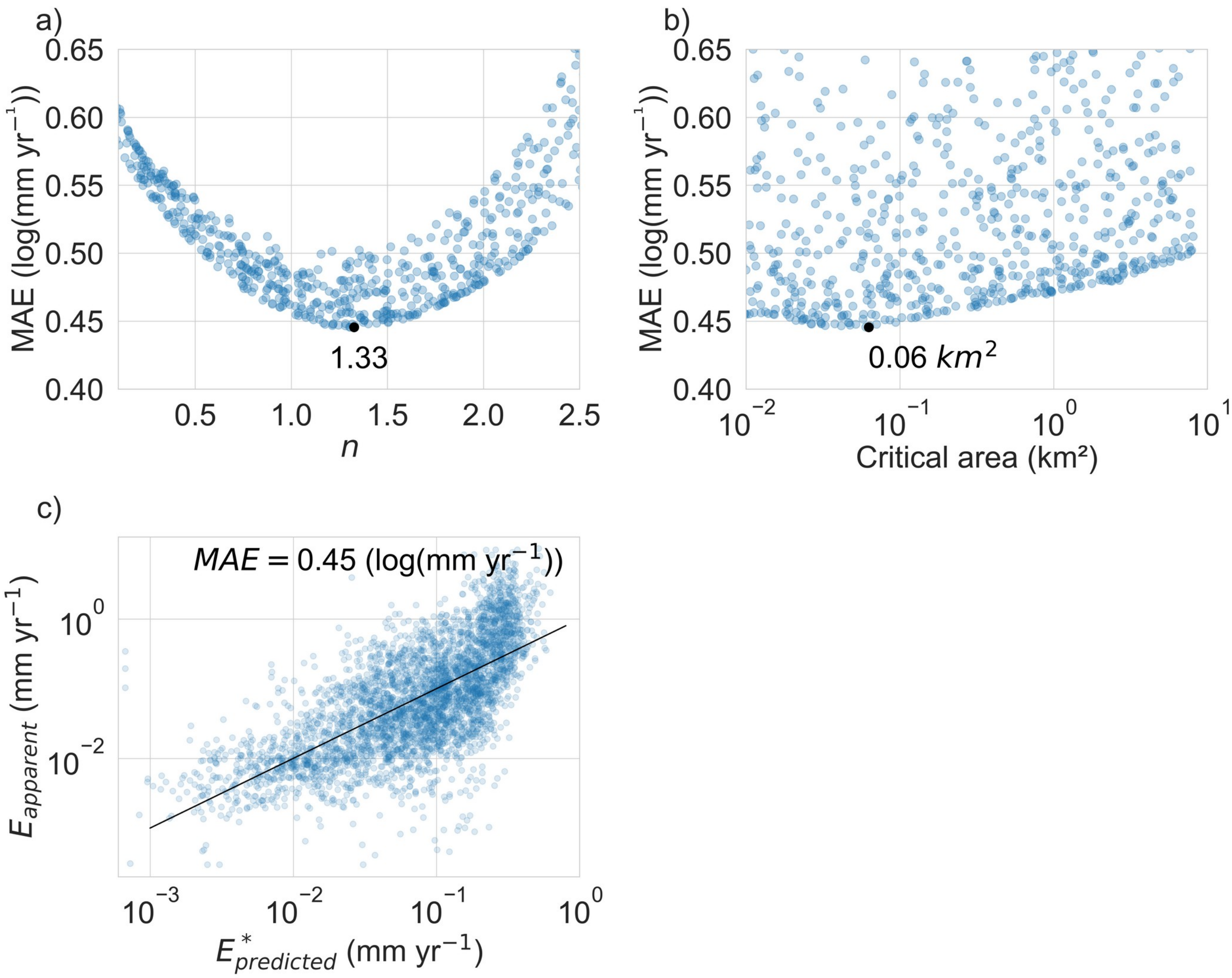

Figure B1: The optimal advection-only values, using MAE as a likelihood function a) n = 1.33 and b) A_c = 0.06 km^2 are nearly identical to the results from models optimised with r^2 of n = 1.33 and A_c = 0.06, respectively. The optimal model (c) has an average absolute error of 0.45 (log (mm yr^{-1}))

https://doi.org/10.5194/esurf-2022-54
Preprint. Discussion started: 8 November 2022

Earth Surface Dynamics Discussions Open Access EGU

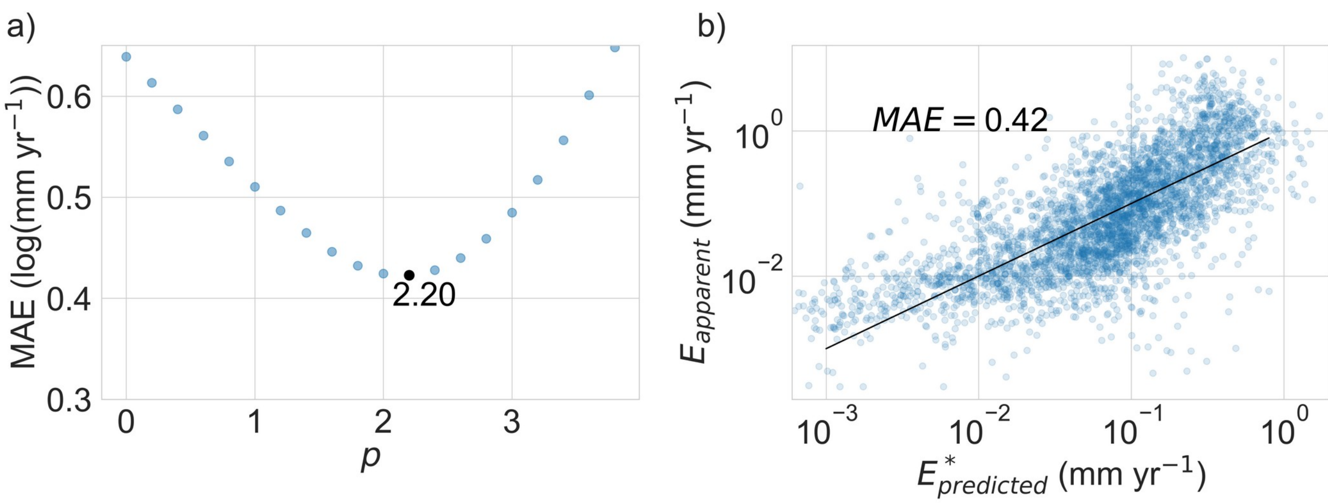

650

Figure B2: a) The optimal diffusion exponent (p) as determined from MAE as a likelihood function is similar to the optimal value using r^2 (2.2 vs 2.0) and gives a minimum error of 0.42 log (mm yr^{-1}).

https://doi.org/10.5194/esurf-2022-54
Preprint. Discussion started: 8 November 2022

Earth Surface Dynamics Discussions
Open Access

Appendix C: Coefficient analysis without bias correction

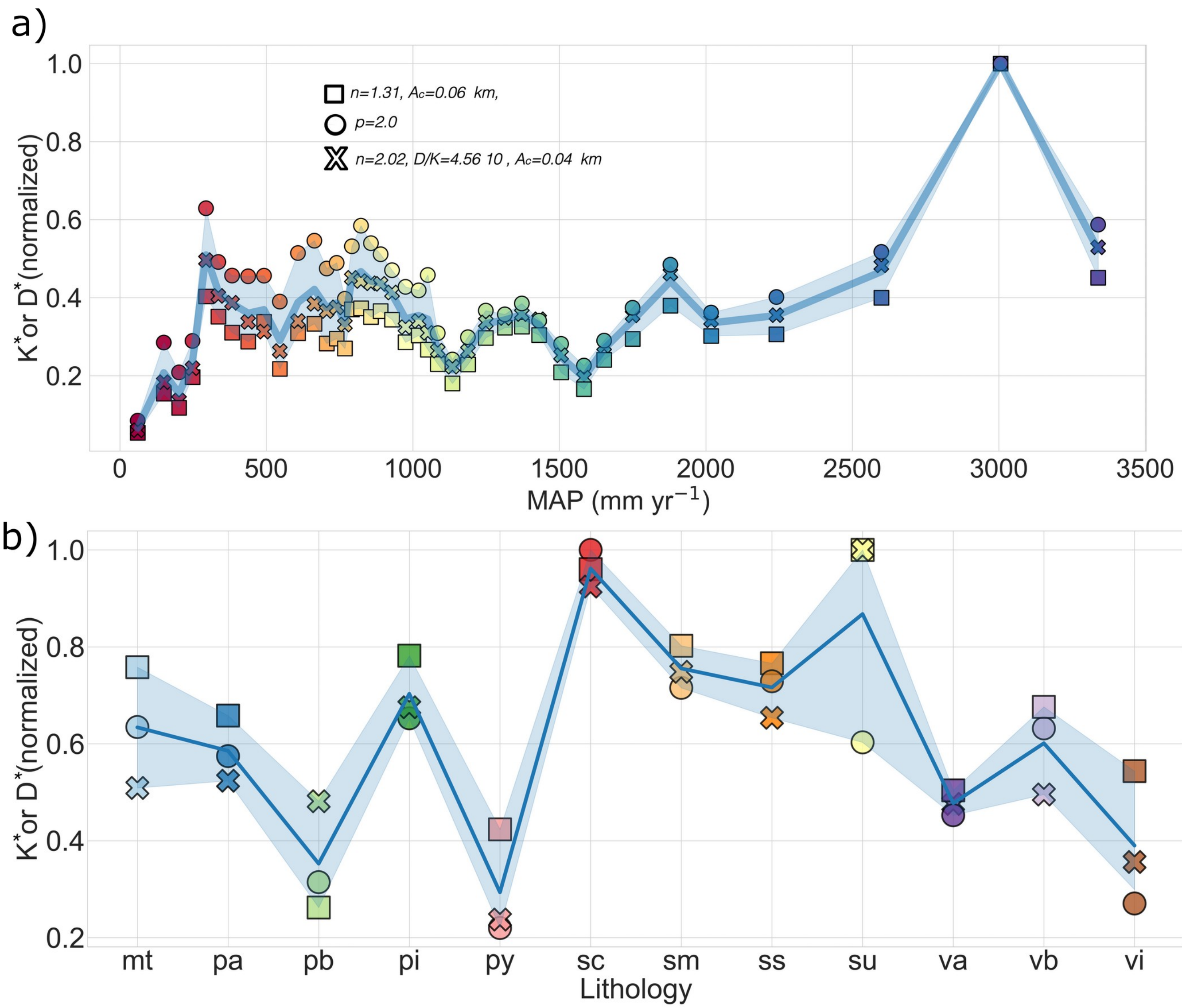

Figure C1: Non-log-transformed coefficients display similar trends with respect to precipitation (a) and lithology (b). The most notable difference between panel a) and Figures 5b is that the un-transformed coefficients display a larger peak at 800 mm yr^{-1}, and a smaller peak at 300 mm yr^{-1}. Few differences are seen for lithological bins, although the maxima (ss and sc) are closer aligned.